HHS Public Access

Author manuscript

Mol Cancer Ther. Author manuscript; available in PMC 2018 December 01.

Published in final edited form as:

Mol Cancer Ther. 2017 December ; 16(12): 2892–2901. doi:10.1158/1535-7163.MCT-17-0170.

Pathway-enriched gene signature associated with 53BP1 response to PARP inhibition in triple-negative breast cancer

Saima Hassan[1,2], **Amanda Esch**[1,*], **Tiera Liby**[1], **Joe W. Gray**[1], and **Laura M. Heiser**[1]

[1]Department of Biomedical Engineering, OHSU Center for Spatial Systems Biomedicine, Oregon Health and Science University

[2]Division of Surgical Oncology, Department of Surgery, Centre Hospitalier de l'Université de Montréal (CHUM), Centre de Recherche du CHUM, l'Université de Montréal, Québec, Canada

Abstract

Treatment of patients with triple negative (ER-negative, PR-negative, HER2-negative) breast cancer remains a challenge. Although PARP inhibitors are being evaluated in clinical trials, biomarkers are needed to identify patients that will most benefit from anti-PARP therapy. We determined the response of three PARP inhibitors: veliparib, olaparib, and talazoparib in a panel of eight triple-negative breast cancer cell lines. Therapeutic responses and cellular phenotypes were elucidated using high-content imaging and quantitative immunofluorescence to assess markers of DNA damage (53BP1) and apoptosis (cleaved-PARP). We determined the pharmacodynamic changes in percentage of cells positive for 53BP1, mean number of 53BP1 foci per cell, and percentage of cells positive for cleaved-PARP. Inspired by traditional dose-response measures of cell viability, an EC50 value was calculated for each cellular phenotype for each PARP inhibitor. The EC50 values for both 53BP1 metrics strongly correlated with IC50 values for each PARP inhibitor. Pathway enrichment analysis identified a set of DNA repair and cell cycle associated genes that were associated with 53BP1 response following PARP inhibition. The overall accuracy of our 63 gene set in predicting response to olaparib in seven breast cancer patient-derived xenograft tumors was 86%. In triple-negative breast cancer patients not treated with anti-PARP therapy, the predicted response rate of our gene signature was 45%. These results indicate that 53BP1 is a biomarker of response to anti-PARP therapy in the laboratory, and our DNA damage response gene signature may be used to identify patients who are most likely to respond to PARP inhibition.

Keywords

triple-negative breast cancer; PARP inhibition; DNA damage response; high-content imaging; genes and pathways

Corresponding Authors: Saima Hassan, MD, PhD, FRCSC, CRCHUM, 900 St. Denis Street, Pavilion R, R10.422, Montréal, Québec, H2X 0A9, Phone: (514) 890-8000; ext. 25497, saimanoorhassan@gmail.com, Laura M. Heiser, PhD, Oregon Health and Science University, 2730 SW Moody Ave., CL3G, Portland, OR 97201-5042, USA, Phone: (503) 346-4617, heiserl@ohsu.edu.

*Current affiliation: Fluidigm, Toronto, Canada

Introduction

Although the overall survival of patients with breast cancer has improved over the past two decades (1), patients with triple-negative breast cancer have a poor prognosis with shorter disease-free survival and overall survival (2). Lacking expression of estrogen receptor, progesterone receptor, and HER2, triple-negative breast tumors constitute 15–20% of all breast cancers, are genomically and phenotypically heterogeneous, and have few effective therapeutic options (3). One of the strongest risk factors that have been identified for developing triple-negative breast cancer is a deleterious mutation in the *BRCA1* gene, which is present in 10–15% of patients with triple-negative breast cancer (4). One family of targeted therapeutic agents that have shown promise for patients with *BRCA1/2* mutations and triple-negative breast cancer are PARP (Poly-ADP Ribose Polymerase) inhibitors (5).

PARP inhibitors have two main mechanisms of action: synthetic lethality, and PARP-DNA trapping. The underlying premise for synthetic lethality is that of a two-hit theory; PARP inhibition in combination with defective *BRCA1/2* function results in complex chromatid rearrangements and ultimately, cell death (6,7). PARP inhibitors target PARP1, an enzyme when recruited to single-strand breaks, binds to DNA, and catalyzes the synthesis of PARP chains onto a series of protein substrates (PARylation). In this process, PARP1 recruits DNA repair proteins and eventually autoPARylates, leading to its release from damaged DNA. PARP inhibitors also have been shown to trap PARP1/2 enzymes on damaged DNA, creating trapped PARP-DNA complexes that induce cytotoxicity (8,9).

Several PARP inhibitors are currently undergoing testing in the preclinical and clinical settings. We focus here on three PARP inhibitors: veliparib (ABT-888, Abbvie), olaparib (AZD2281, AstraZeneca), and talazoparib (Pfizer, formerly called BMN 673). While all three PARP inhibitors are orally available and have been shown to target PARP1/2 activity, talazoparib has demonstrated the greatest potency in trapping PARP-DNA complexes (8–10). Over 100 clinical trials have been undertaken with PARP inhibitors, with the greatest emphasis on patients with *BRCA1/2* mutations (10). Of these three PARP inhibitors, olaparib is the most advanced in its clinical development, having been granted FDA approval for use in ovarian cancer (11). Current clinical trials are testing PARP inhibitors as a single agent and in combination with other therapeutic agents in patients with triple-negative breast cancer and other types of cancers (10,12).

Our goal in this study was to identify pharmacodynamic biomarkers of response and genes that will predict response to PARP inhibitors. We accomplished this by assessing responses in a panel of well-characterized triple-negative breast cancer cell lines to three PARP inhibitors and correlating these responses with molecular features measured from the cell lines. In our study, we used high content imaging (13,14) to measure cellular changes in DNA damage and cell death in response to PARP inhibition. We found the DNA damage response to correlate strongly with IC50 values, and identified the genes and critical pathways associated with DNA damage response to PARP inhibition. Finally, we validated the predictive value of our gene signature in a publically available dataset of patient-derived xenografts, and identified the clinical relevance of these genes in breast cancer patients with triple-negative disease.

Materials and Methods

In-vitro drug sensitivity assay

We first performed experiments to identify optimal cell seeding densities to ensure an average of 75% confluence of control cells at the end of the assay. Cells were assessed in a 96-well plate format, where each plate tested two drugs, and 9 concentrations of each drug that were distributed in a randomized layout. Perimeter wells were not used. We tested each concentration in triplicate wells and in one to three replicate assays. Cells were plated and allowed to adhere for 24 hours, followed by drug treatment (Fig. 1). Media and drug were changed after 4–5 days. For all experiments, cells were treated for 10 days. After 10 days, cells were fixed and permeabilized with 4% paraformaldehyde, diluted from stock Paraformaldehyde 32% Solution, EM Grade (Cat No. 15714, Electron Microscopy Sciences), and 0.3% Triton X-100 (Cat No. T9284, Sigma-Aldrich).

We tested three PARP inhibitors: veliparib, olaparib, and talazoparib (Selleckchem, Cat Nos. S1004, S1060, S7048, respectively). Chemical formulations can be found in Fig. 2A–C. We used 1:5 serial dilutions, with concentrations optimized for each compound: veliparib and olaparib tested at 0.25 nM to 100 μM; and talazoparib, tested at 0.0128 nM to 5 μM.

We studied eight molecularly-characterized triple-negative breast cancer (TNBC) cell lines from our laboratory (15): MDAMB436, MDAMB231, MDAMB453, MDAMB468, HCC1143, HCC1937, HCC1806, and HCC1395 (Supplementary Table S1). Short tandem repeat (STR) DNA profiling (Genetica DNA Laboratories, Burlington, NC) performed in October 2014 prior to conduction of chemosensitivity experiments, confirmed cell line authenticity, and PCR analysis verified the absence of Mycoplasma. Molecular features of the cell lines, including gene cluster information (15,16), breast cancer subtype (15,17), mutational status for *BRCA1/2, ATM, ATR* (18,19), and *PTEN* deficiency status (20), are summarized in Supplementary Table S1.

Immunofluorescence

We prepared a primary and secondary antibody solution using 2% Bovine Serum Albumin (Cat No. 001-000-162, Jackson Immunoresearch). We used the following primary antibodies: cleaved-PARP (cl-PARP) (1:200, Cat No. 9546, Cell Signaling Technology) and 53BP1 Antibody (1:500, Cat No. NB100-904, Novus Biologicals). Secondary antibodies used were: Alexa 488 donkey anti-mouse (1:300, Cat No. A21202, Life Technologies) and Alexa 647 donkey anti-rabbit (1:300, Cat No. A31573, Life Technologies). We used HCS Nuclear Mask (1:2000, Cat No. H10325, Life Technologies) to stain the nucleus, which was added at the time of the secondary antibody solution.

High-content imaging

We performed wide-field microscopy using a scan^R microscope (Olympus, Germany) alongside an ORCA-R^2 CCD Digital Camera (Hamamatsu, Japan) (21) with a 10× objective and filter sets for Alexa 488 and Alexa 647. We scanned 25 images per well and performed image analysis with spot identification using scan^R analysis software version 2.4.1.1.

Statistical analysis for immunofluorescence: We analyzed the DMSO control wells to identify the baseline level of 53BP1 foci per nucleus and cl-PARP intensity for each cell line.

We calculated two metrics for 53BP1: 1) percentage of cells positive for 53BP1 foci formation; and 2) mean number of 53BP1 foci per nucleus. In the control cells, we identified the number of foci at the 95^{th} percentile, such that 5% of cells were considered positive for 53BP1 foci formation. We used these thresholds to identify the percentage of positive cells for 53BP1 foci formation for each drug concentration of each cell line. We also determined the mean number of 53BP1 foci per nucleus for each drug concentration of each cell line.

We used a similar approach to analyze the cl-PARP intensity signal. Here, the 99th percentile of the intensity cl-PARP in the DMSO control cells was used to threshold cells into positive and negative bins. Cells positive for cl-PARP expression were interpreted to be apoptotic. The threshold of 1% was chosen based on what was previously reported (22), and was kept constant across all cell lines. We also calculated the percentage of apoptotic cells for each drug concentration. All single-cell analysis was performed using STATA SE (version 13.1, Statacorp, Texas).

Data visualization

For each PARP inhibitor concentration, we created heatmaps to visualize three metrics: 1) percentage of cells positive for 53BP1, 2) mean number of 53BP1 foci per nucleus; 3) percentage of cells positive for cl-PARP. In all cases, data from each drug treatment were normalized to the DMSO control. Values were scaled to the maximum value to compare across cell lines. Heatmaps were created using Multi Experiment Viewer (MeV) software (23). A double gradient color scheme was used, where 10% of the elements were at the lowest and highest levels of color saturation.

Calculation of EC50 curves: We calculated EC50 cells for each of the following cellular phenotypes: percentage of cells positive for 53BP1, mean number of 53BP1 foci per cell, and percentage of cells positive for cl-PARP. EC50 is defined as the drug concentration required to induce a response halfway between the baseline and maximum response. For each phenotype, we normalized the values for each well of each drug concentration by subtracting the mean value of triplicate wells for the DMSO control. We divided the normalized values for each drug concentration by the maximal value (mean of triplicate wells). These normalized metrics were plotted against the log-transformed molar drug concentrations with a top constraint of 100. We fit a sigmoidal curve to these data and interpolated to identify the drug concentration at 50% of the maximal response. Spearman's rank correlations were used to correlate EC50 values with IC50 values. EC50 values and correlations were calculated using Graph Pad Prism (version 6.0d for Mac OS X, Graph Pad Software, California).

Cell cycle analysis

We determined the cell cycle distribution of DNA content by analyzing frequency histograms of total DAPI intensity. We first set up gates in the control (DMSO) population of each plate, and then these gates were applied to each treatment well. Constraints were

applied to the mean peak population of 2N and 4N, and to the coefficient of variation, such that the coefficient of variation of 4N was set at the same as 2N. We reported the results of cell cycle analysis when cell numbers per well were greater than 200. We performed all cell cycle analysis using FlowJo (v10.1r5, Oregon).

Gene association analysis

We identified genes associated with the 53BP1 response and assessed their clinical significance using the pipeline described in Figure S1. For this analysis, we stratified the cell lines into two groups: sensitive and resistant to PARP inhibition using the percentage of cells positive for 53BP1 response. The PARP inhibitors were grouped to determine the three common sensitive cell lines and three common resistant cell lines. We used previously published gene expression data from untreated cell lines (15) and calculated a log fold-change metric by dividing the average gene expression of the sensitive cell lines by the average gene expression of the resistant cell lines to create a rank list. We also created a curated list of gene sets from gene sets previously shown to be implicated in predicting response to olaparib (20,24), talazoparib (25), BRCAness (26), *BRCA1* (27), *BRCA2* (27), homologous recombination deficiency (HRD) (28), and DNA damage response pathways (29). We used our rank gene list and the curated gene set list to perform a preranked gene set enrichment analysis (GSEA) to identify enriched gene sets and core enriched genes. There are four statistical parameters that are used to describe and interpret the GSEA output. The *normalized enrichment score (NES)* reflects the degree to which a gene set is overrepresented at the top or bottom of a ranked list of genes, taking into account differences in gene set size. The *nominal p-value* represents the statistical significance of the enrichment score for a single gene set. The *false discovery rate (FDR)* is the estimated probability for a false positive finding of a gene set with a given NES. FDR is adjusted for gene set size and multiple hypothesis testing. The *rank metric score* is the position of the gene in the ranked list of genes. GSEA was performed using GenePattern (Version 3.9.8, Build Id: 140) (30).

To determine which pathways were statistically associated with the core genes, Reactome Pathway Enrichment analysis was performed within Cytoscape v3.3.0. We identified enriched pathways and the genes associated with these pathways, with an FDR q-value < 0.1. The pathways were organized into their hierarchy of major, minor, subpathways, and components, based on the hierarchical organization provided by Reactome within Cytoscape. We considered a pathway to be significant only if the major or minor pathways were statistically significant (FDR q-value < 0.1).

We evaluated the clinical significance of our 63 pathway-enriched genes by assessing their frequency of mutation in triple-negative breast cancer patients (n=82), and ER-positive patients (n=594) from The Cancer Genome Atlas (TCGA dataset) (31) available in cBioPortal (32). Mutation frequency was also assessed in breast cancer patients with the following subtypes: basal (n = 81), luminal B (n=133), and luminal A (n = 235) (33).

We tested the predictive potential of our gene signature using previously published expression data of seven breast cancer tumors that were treated with olaparib in a patient-derived xenograft (PDX) model (34). We normalized the gene expression data as previously described (20) and used a weighted voting algorithm (30). Sensitivity and resistance to

olaparib was defined as per Bruna et al (34). We also determined the performance of previously published gene signatures predictive of response to PARP inhibition or BRCAness (20,24–28) with treatment to olaparib in patient-derived xenografts. For each of the gene signatures, our 53BP1 cell-line response was used to train the response to PARP inhibition, and a weighted voting algorithm was used to predict response in mice. Parameters that were used to compare performance of gene signatures include: overall accuracy ((true positives + true negatives)/(true positives + false positives + true negatives + false negatives)), sensitivity, specificity, positive predictive value, negative predictive value, and a positive test, referring to the sum of tumors wherein the test was sensitive to olaparib.

We also determined the predictive potential of our gene signature and those previously published in a cohort of 82 triple-negative breast cancer patients from TCGA. We obtained FPKM-upper quartile normalized gene expression data from the NCI Genomic Data Commons portal (35), and processed the data as previously described (20). Prediction of response to PARP inhibition was calculated using the same weighted voting algorithm that was used to predict response in the PDX model (30,36). The prediction of response or sensitivity to PARP inhibition was defined as a positive test.

Results

Talazoparib has greater potency in triple-negative breast cancer cell lines than veliparib or olaparib

We used a 10-day assay to measure responses of eight TNBC cell lines to three PARP inhibitors (Fig.2, Supplementary Fig. S2, Supplementary Tables S1 and S2). As expected, the two most sensitive cell lines, MDAMB436 and HCC1395, were $BRCA^{MUT}$ (BRCA mutant) and the most resistant cell line, HCC1143, was $BRCA^{WT}$ (BRCA wild-type) (Fig. 2D and Supplementary Fig. S2). Talazoparib demonstrated the greatest potency, with mean IC50 values ranging between 0.20 nM and 28.0 nM. Olaparib IC50 values ranged from 0.003 μM to 3.8 μM, while IC50 values for veliparib varied between 0.03 μM and 67.1μM. Olaparib is 5–50 fold more potent than veliparib, and talazoparib is 15–170 fold more potent than olaparib, depending on the cell line (Supplementary Table S3).

To better understand the significance of the IC50 values in the context of patients, we annotated Fig. 2D with the plasma concentrations achieved in patients for each compound. We obtained the peak plasma concentrations of each compound within 24 hours of drug administration from clinical trials. The average plasma concentrations described in the literature are: 9.9 μM for veliparib (37,38), 14 μM for olaparib and 25 nM for talazoparib (39,40). Therefore, the IC50 values for olaparib and talazoparib were mainly at physiologic concentrations, whereas the IC50 values for veliparib exceeded the maximum plasma concentrations for three of the eight cell lines.

Variability in DNA damage response and apoptosis across cell lines and PARP inhibitors

We examined the DNA damage response, represented by 53BP1 foci formation following treatment with each PARP inhibitor (Fig. 3A–C, Supplementary Fig. S3). We observed variability in the number of 53BP1 foci across cell lines, with greater number of foci in

HCC1806, and the fewest foci in HCC1143. Treatment with olaparib or talazoparib also resulted in cells with larger nuclei in the HCC1806 and MDAMB231 cell lines, as compared to HCC1143. Our imaging approach allowed us to quantitatively compare the effect of PARP inhibition on cell cycle and hyperploid cell populations (Supplementary Figs. S4 and S5). In comparison to HCC1143, increasing concentrations of all three PARP inhibitors was associated with an increasingly greater proportion of hyperploid cells in MDAMB231 and HCC1806 cell lines. Since HCC1806 is much more sensitive to PARP inhibition than MDAMB231 and HCC1143, it is plausible that an increase in DNA content is associated with response to PARP inhibition. Treatment with olaparib or talazoparib was also associated with a greater proportion of cells undergoing apoptosis, in comparison to veliparib (Fig. 3D–E, Supplementary Fig. S6).

Strong correlation between EC50 values for 53BP1 response and IC50 values

We calculated EC50 values for each of the phenotypic endpoints: percentage of cells positive for 53BP1, number of 53BP1 foci per cell, and percentage of cells positive for cl-PARP (Supplementary Figs. S7 and S8). Overall, the EC50 values for 53BP1, computed from both percentage of cells and mean number of foci, demonstrated a similar trend across all the cell lines. The EC50 values for percentage of cells positive for cl-PARP were generally higher than the IC50 values. We performed correlations between IC50 and EC50 values for each PARP inhibitor. Supplementary Fig. S9 shows statistically significant correlations for each of the PARP inhibitors between IC50 and EC50 values for percentage of cells positive for 53BP1 for veliparib (r = 0.83, $P = 0.01$), olaparib (r = 0.96, $P = 0.003$), and talazoparib (r = 0.93, $P = 0.002$). We also identified positive correlations between IC50 and EC50 values for 53BP1 foci for veliparib (r = 0.95, $P = 0.001$), olaparib (r = 0.93, $P = 0.007$), and talazoparib (r = 0.83, $P = 0.01$). There were no statistically significant correlations between IC50 values and EC50 values for percentage of cells positive for cl-PARP.

We determined the dose dependent effect of veliparib, olaparib, and talazoparib upon percent cells positive for 53BP1, mean number of 53BP1 foci per cell, and percentage of cells positive for cl-PARP (Fig. 4). For the two 53BP1 metrics (Fig. 4A,B), we see a shift in the response from veliparib to olaparib to talazoparib, with increased 53BP1 foci formation or percentage of cells positive for 53BP1 at progressively lower concentrations for all cell lines. Since the concentration range tested was in the same micromolar range for veliparib and olaparib, while the concentration range for talazoparib was mainly in the nanomolar range, this suggests that the 53BP1 response is similar across all three PARP inhibitors, but the differences observed may be attributed to differences in affinity between the PARP inhibitors. Fig. 4C shows the dose response of each PARP inhibitor upon apoptosis. The effect is more dichotomous, and the induction of apoptosis occurs near the peak plasma concentrations observed in patients.

Gene association analysis of 53BP1 response

One of our aims was to identify a set of genes that was associated with response to all three PARP inhibitors (Supplementary Fig. S1). We created a transcriptome-wide ranked list of differential gene expression between the sensitive and resistant cell lines (Supplementary

File 1). This ranked gene list was used in a GSEA analysis to assess whether gene sets previously shown to be involved with response to PARP inhibition, BRCAness, *BRCA1*/*2* mutation status, HRD, or DNA damage repair (20,24–28) are differentially expressed in sensitive and resistant cell lines (see Supplementary File 2 for gene set lists). The total number of genes from these lists is 1091, of which there are 919 unique genes. Six of the eight gene sets were significantly differentially expressed between sensitive and resistant cell lines at q-value < 0.25 (Supplementary Figure S10A, S11). Significant gene sets include the two olaparib associated gene sets, *BRCA1* and *BRCA2* signatures, BRCAness, and the HRD signature. These gene sets have a negative enrichment score, which indicates that their downregulation is associated with sensitivity to PARP inhibition. We identified 189 core-enriched genes, (Supplementary File 3), of which, twelve of these genes were present in more than two or three gene sets: *MCM2, RAD51C, HELLS, ESCO2, TIMELESS, NBN, BRCA1, MCM3, ATAD5, ANLN, FAM83D*, and *SHCBP1* (Supplementary Figure S10B). Since these genes were derived from two or three different independent methods, we consider these genes to be of high interest.

We were also interested in determining the pathways enriched in the 176 core genes associated with response to PARP inhibition. Using Reactome pathway enrichment analysis, we identified three major pathways: DNA repair, cell cycle, and programmed cell death (Table 1, Supplementary File 4). Major and minor pathways have been defined above in the Materials and Methods section. Within the major pathway of DNA repair, several minor pathways involved in single-strand break and double-strand break repair were identified including base excision repair, nucleotide excision repair, mismatch repair, and homology-directed repair. Of note, genes implicated in DNA damage bypass, such as translesion synthesis were also enriched. Cell cycle genes were also enriched, including checkpoint factors, as well as genes involved in DNA replication, chromosome maintenance, and telomere maintenance.

Clinical significance of pathway enriched genes

From the list of enriched major and minor pathways, we identified a unique set of 63 genes. Because inactivation of DNA damage response pathways typically leads to increased genomic instability (29), we analyzed the frequency with which these genes are mutated (including truncating, inframe and missense mutations) in different breast cancer subtypes using patient datasets from TCGA (31,33) within cBioPortal (32) (Supplementary Fig. S12A). As expected, the mutational frequency of these genes was enriched in patients with triple-negative, basal breast cancer or ER-negative breast cancers (Supplementary Fig. S12B). 85% of the patients with triple-negative breast cancer demonstrated a mutation in these genes, and in total we observed mutations in 21 of the 63 genes were mutated. This contrasts with a frequency of 31% for patients with ER-positive disease (31). The trend for this mutational frequency was also present in the intrinsic subtypes: 90% for basal, 38% for luminal B, and 17% for luminal A subtypes (33).

It is plausible that synergy with anti-PARP therapy may be achieved by targeting members of DNA repair or other DNA damage response pathways. Possible druggable targets of the DNA damage response pathways was extensively reviewed previously using several

approaches including targets with druggable structures, ligand-based approach, network-based approach, and based on the availability of compounds of submicromolar activity or affinity (29). We found that 19 of the 21 mutated genes demonstrated druggable potential and are candidates for co-treatment with PARP inhibitors (Supplementary Table S4) (29).

Predictive performance of our gene signature

We determined the predictive value of our gene signature in patient-derived xenografts treated with olaparib using previously published data of seven breast cancer tumors (34). Three of these tumors were $BRCA1^{MUT}$, of which 2 were sensitive to olaparib and 1 was resistant. The clinical characteristics of these tumors were previously reported (34). We found that our combined PARP inhibitor gene signature correctly predicted response in 6/7 tumors. Our signature performed comparably to olaparib (24), talazoparib (25) and HRD (28) gene signatures, which predicted response in 5/7 tumors, and better than the gene signatures associated with BRCA1/2 mutations (27), which demonstrated a poorer specificity (Table 2).

We also determined the predictive value of the gene signatures in 82 triple-negative breast cancer patients from TCGA that were not reported to receive anti-PARP therapy (Table 2). Our combined PARP inhibitor gene signature predicted that 45% of triple-negative breast cancer patients would respond to anti-PARP therapy. Overall, the predicted response rate in TNBC patients was similar to the frequency of a positive test identified *in-vivo*. Because the patient TCGA cohort did not receive anti-PARP therapy, false positives could not be identified, and so our prediction of response rate is not a reflection of overall accuracy.

Discussion

The efficacy of PARP inhibitors in cell lines has been previously published using different approaches, with varying assay lengths – from 72 hours to 15 days, and different measurements of cell viability, such as sulforhodamine B or Alamar Blue (resazurin) (17,20,41). We used an automated approach to measure nuclear counts as a rapid and more direct means of determining therapeutic response after ten days of treatment. In the context of triple-negative breast cancer, we found that talazoparib had the greatest potency, with IC50 values in the nanomolar range, followed by olaparib and veliparib, with IC50 values in the micromolar range. We also found that talazoparib was about 100-fold more potent than olaparib, in terms of IC50 values in most of the cell lines. Since talazoparib was previously shown to be 100-fold more potent than olaparib at trapping PARP-DNA complexes (9), it is plausible that the PARP-trapping mechanism is mainly responsible for talazoparib's greater potency in therapeutic response.

Our study is the first to use high content imaging to demonstrate heterogeneity in expression of 53BP1 and the apoptosis across multiple breast cancer cell lines. Although semi-quantitative and manual approaches have been previously used to measure the level of double-strand or single-strand breaks (42), and to identify the percentage of cells that express γ-H2AX or 53BP1 in response to PARP inhibition (25,43), high-content imaging allows screening of several cell lines and drug concentrations in a high-throughput manner and single cell-analysis. We found that the EC50 values of 53BP1 foci formation or

percentage of cells positive for 53BP1 strongly correlated with IC50 values, suggesting the significance of the DNA damage response as a phenotypic endpoint. Of note, we did not identify a statistically significant correlation between the EC50 values for apoptosis and any of the three PARP inhibitors. This could be due to the presence of alternative mechanisms of cell death, such as mitotic catastrophe, for example, which may result from an accumulation of chromatid aberrations.

Although clinical trials have focused on patients with *BRCA1/2* mutations, the search for predictors of BRCAness for breast cancer tumors is ongoing (10). A vast array of methodologies has been used to identify gene signature predictors of response to PARP inhibitors or BRCAness. These include genetic screens using siRNA/shRNA libraries (24,25,28), and computational approaches using *in vitro* response and genes that were previously known to be involved in DNA repair (20). Gene signatures for BRCAness, *BRCA1* and *BRCA2*, have also been derived from breast cancer or ovarian cancer patients without any prior selection for genes involved with DNA repair (26,27). Our novel approach of comparing the 53BP1 response in sensitive and resistant cell lines provides insight into the pathways associated with response to the three PARP inhibitors.

Our core gene set enrichment analysis identified some of the critical genes previously found to be important in determining response to PARP inhibition. For example, Daemen et al. (20) identified 5 genes associated with response to olaparib, namely, *BRCA1, NBN, TDG, XPA*, and *MRE11A*. Interestingly, we also identified CDK12 to be a core-enriched gene from Bajrami et al.'s gene set (24), which has been shown to play a role in resistance to PARP inhibition (44).

We identified key pathways associated with response to PARP inhibition using pathway enrichment analysis. In addition to DNA repair pathways, we also found other pathways involving translesion synthesis, telomere maintenance, as well as cell cycle and checkpoint factors associated with response to PARP inhibition. This is not surprising as genes associated with transcription, chromatin modification, mitosis, and apoptosis have previously been reported to be associated with PARP function (10). Furthermore, pathways involving translesion synthesis, telomere maintenance and checkpoint factors, have all been shown to be important components of the DNA damage response pathways (29).

We determined the clinical significance of the pathway-enriched genes in breast cancer patients. We found an enrichment in the mutational frequency of our 63 genes in basal and triple-negative breast cancers in comparison to Luminal A, and ER-positive breast cancers, suggesting that our panel of breast cancer cell lines is representative of the genetic aberrations in triple-negative breast cancer patients. This is concordant with what we and others previously demonstrated, in that panels of breast cancer cell lines capture much of the genomic, transcriptomic and biological heterogeneity of primary breast tumors (16,45), and can be used to demonstrate a differential response to therapy (15). We also identified druggable potential of most of the mutated genes, suggesting the possibility for identifying novel therapeutic agents that could be used in combination with anti-PARP therapy.

We further validated our combined PARP inhibitor gene signature on patient-derived breast cancer xenografts and found that the overall accuracy of our gene signature in predicting response to olaparib was 86% in seven tumors. Although there were a small number of tumors in this validation cohort, we still compared the performance of other BRCAness gene signatures. We found that our gene signature was one of the higher performing signatures. We also determined the predicted response rate of our combined PARP inhibitor gene signature to be 45% in triple-negative breast cancer patients.

In summary, we used high content cell-imaging to determine chemosensitivity of PARP inhibitors in a panel of eight breast cancer cell lines. We identified a novel approach to characterize the DNA damage and cell death response. Using gene set and pathway enrichment analysis, we identified gene predictors of 53BP1 response to PARP inhibition. When mutated, these genes are prevalent in triple-negative breast cancer patients, and are suggestive of druggable targets that could be used in combination with anti-PARP therapy. The high overall accuracy of our gene signature in patient-derived xenografts and predicted response rate in triple-negative breast cancer patients leads the way for clinical studies to validate the predictive potential of our gene signature in triple-negative breast cancer patients.

Supplementary Material

Refer to Web version on PubMed Central for supplementary material.

Acknowledgments

This study was conducted with salary support from the Canadian Breast Cancer Foundation, Banting Postdoctoral Fellowship administered by the Canadian Institutes of Health Research, Ontario Institute for Cancer Research by the Government of Ontario, and grant support from Young Investigator Award by the Conquer Cancer Foundation of ASCO, the Evelyn H. Lauder Family, and the Breast Cancer Research Foundation (SH), and by the National Institutes of Health, National Cancer Institute grant U54 CA 112970 (JWG). SH would also like to acknowledge her mentor, Dr. André Robidoux, members of her division of Surgical Oncology at the CHUM, and l'Institut de Cancer de Montréal.

References

1. Howlader, N., Noone, AM., Krapcho, M., Garshell, J., Miller, D., Altekreuse, SF., et al. SEER Cancer Statistics Review, 1975–2012. Vol. 2015. Bethesda, MD: National Cancer Institute; Apr. 2015 posted to the SEER web site
2. Anders CK, Carey LA. Biology, metastatic patterns, and treatment of patients with triple-negative breast cancer. Clin Breast Cancer. 2009; 9(Suppl 2):S73–81. DOI: 10.3816/CBC.2009.s.008 [PubMed: 19596646]
3. Metzger-Filho O, Tutt A, de Azambuja E, Saini KS, Viale G, Loi S, et al. Dissecting the heterogeneity of triple-negative breast cancer. Journal of clinical oncology : official journal of the American Society of Clinical Oncology. 2012; 30(15):1879–87. DOI: 10.1200/JCO.2011.38.2010 [PubMed: 22454417]
4. Gonzalez-Angulo AM, Timms KM, Liu S, Chen H, Litton JK, Potter J, et al. Incidence and outcome of BRCA mutations in unselected patients with triple receptor-negative breast cancer. Clinical cancer research : an official journal of the American Association for Cancer Research. 2011; 17(5): 1082–9. DOI: 10.1158/1078-0432.CCR-10-2560 [PubMed: 21233401]
5. Rugo HS, Olopade OI, DeMichele A, Yau C, van 't Veer LJ, Buxton MB, et al. Adaptive Randomization of Veliparib-Carboplatin Treatment in Breast Cancer. The New England journal of medicine. 2016; 375(1):23–34. DOI: 10.1056/NEJMoa1513749 [PubMed: 27406347]

6. Lord CJ, Ashworth A. Mechanisms of resistance to therapies targeting BRCA-mutant cancers. Nature medicine. 2013; 19(11):1381–8. DOI: 10.1038/nm.3369
7. Lord CJ, Tutt ANJ, Ashworth A. Synthetic Lethality and Cancer Therapy: Lessons Learned from the Development of PARP Inhibitors. Annual Review of Medicine. 2015; 66(1):455–70. DOI: 10.1146/annurev-med-050913-022545
8. Murai J, Huang S-yN, Das BB, Renaud A, Zhang Y, Doroshow JH, et al. Trapping of PARP1 and PARP2 by Clinical PARP Inhibitors. Cancer Research. 2012; 72(21):5588–99. DOI: 10.1158/0008-5472.can-12-2753 [PubMed: 23118055]
9. Murai J, Huang S-YN, Renaud A, Zhang Y, Ji J, Takeda S, et al. Stereospecific PARP Trapping by BMN 673 and Comparison with Olaparib and Rucaparib. Molecular cancer therapeutics. 2014; 13(2):433–43. DOI: 10.1158/1535-7163.mct-13-0803 [PubMed: 24356813]
10. Sonnenblick A, de Azambuja E, Azim HA Jr, Piccart M. An update on PARP inhibitors[mdash]moving to the adjuvant setting. Nature reviews Clinical oncology. 2015; 12(1): 27–41. DOI: 10.1038/nrclinonc.2014.163
11. Olaparib. [Accessed 2015 07/29/15] U.S. Food and Drug Administration. <http://www.fda.gov/Drugs/InformationOnDrugs/ApprovedDrugs/ucm427598.htm>
12. Mateo J, Carreira S, Sandhu S, Miranda S, Mossop H, Perez-Lopez R, et al. DNA-Repair Defects and Olaparib in Metastatic Prostate Cancer. The New England journal of medicine. 2015; 373(18): 1697–708. DOI: 10.1056/NEJMoa1506859 [PubMed: 26510020]
13. Pepperkok R, Ellenberg J. High-throughput fluorescence microscopy for systems biology. Nat Rev Mol Cell Biol. 2006; 7(9):690–6. [PubMed: 16850035]
14. Perlman ZE, Slack MD, Feng Y, Mitchison TJ, Wu LF, Altschuler SJ. Multidimensional Drug Profiling By Automated Microscopy. Science. 2004; 306(5699):1194–8. DOI: 10.1126/science.1100709 [PubMed: 15539606]
15. Heiser LM, Sadanandam A, Kuo WL, Benz SC, Goldstein TC, Ng S, et al. Subtype and pathway specific responses to anticancer compounds in breast cancer. Proceedings of the National Academy of Sciences of the United States of America. 2012; 109(8):2724–9. DOI: 10.1073/pnas.1018854108 [PubMed: 22003129]
16. Neve RM, Chin K, Fridlyand J, Yeh J, Baehner FL, Fevr T, et al. A collection of breast cancer cell lines for the study of functionally distinct cancer subtypes. Cancer cell. 2006; 10(6):515–27. DOI: 10.1016/j.ccr.2006.10.008 [PubMed: 17157791]
17. Lehmann BD, Bauer JA, Chen X, Sanders ME, Chakravarthy AB, Shyr Y, et al. Identification of human triple-negative breast cancer subtypes and preclinical models for selection of targeted therapies. The Journal of clinical investigation. 2011; 121(7):2750–67. DOI: 10.1172/JCI45014 [PubMed: 21633166]
18. COSMIC, Catologue of Somatic Mutations in Cancer. [2015-08-27] Wellcome Trust Sanger Institute. <http://cancer.sanger.ac.uk/cell_lines>
19. Tomlinson GE, Chen TT, Stastny VA, Virmani AK, Spillman MA, Tonk V, et al. Characterization of a breast cancer cell line derived from a germ-line BRCA1 mutation carrier. Cancer Res. 1998; 58(15):3237–42. [PubMed: 9699648]
20. Daemen A, Wolf DM, Korkola JE, Griffith OL, Frankum JR, Brough R, et al. Cross-platform pathway-based analysis identifies markers of response to the PARP inhibitor olaparib. Breast cancer research and treatment. 2012; 135(2):505–17. DOI: 10.1007/s10549-012-2188-0 [PubMed: 22875744]
21. Rantala J, Kwon S, Korkola J, Gray J. Expanding the Diversity of Imaging-Based RNAi Screen Applications Using Cell Spot Microarrays. Microarrays. 2013; 2(2):97–114. [PubMed: 27605183]
22. Liu T, Yacoub R, Taliaferro-Smith LD, Sun S-Y, Graham TR, Dolan R, et al. Combinatorial Effects of Lapatinib and Rapamycin in Triple-Negative Breast Cancer Cells. Molecular cancer therapeutics. 2011; 10(8):1460–9. DOI: 10.1158/1535-7163.mct-10-0925 [PubMed: 21690228]
23. Saeed AI, Sharov V, White J, Li J, Liang W, Bhagabati N, et al. TM4: a free, open-source system for microarray data management and analysis. Biotechniques. 2003; 34(2):374–8. [PubMed: 12613259]
24. Bajrami I, Frankum JR, Konde A, Miller RE, Rehman FL, Brough R, et al. Genome-wide Profiling of Genetic Synthetic Lethality Identifies CDK12 as a Novel Determinant of PARP1/2 Inhibitor

Sensitivity. Cancer Research. 2014; 74(1):287–97. DOI: 10.1158/0008-5472.can-13-2541 [PubMed: 24240700]

25. Shen Y, Rehman FL, Feng Y, Boshuizen J, Bajrami I, Elliott R, et al. BMN 673, a novel and highly potent PARP1/2 inhibitor for the treatment of human cancers with DNA repair deficiency. Clinical cancer research : an official journal of the American Association for Cancer Research. 2013; 19(18):5003–15. DOI: 10.1158/1078-0432.CCR-13-1391 [PubMed: 23881923]
26. Konstantinopoulos PA, Spentzos D, Karlan BY, Taniguchi T, Fountzilas E, Francoeur N, et al. Gene Expression Profile of BRCAness That Correlates With Responsiveness to Chemotherapy and With Outcome in Patients With Epithelial Ovarian Cancer. Journal of Clinical Oncology. 2010; 28(22):3555–61. DOI: 10.1200/jco.2009.27.5719 [PubMed: 20547991]
27. Larsen MJ, Kruse TA, Tan Q, Laenkholm AV, Bak M, Lykkesfeldt AE, et al. Classifications within molecular subtypes enables identification of BRCA1/BRCA2 mutation carriers by RNA tumor profiling. PloS one. 2013; 8(5):e64268.doi: 10.1371/journal.pone.0064268 [PubMed: 23704984]
28. Peng G, Chun-Jen Lin C, Mo W, Dai H, Park Y-Y, Kim SM, et al. Genome-wide transcriptome profiling of homologous recombination DNA repair. Nat Commun. 2014; 5doi: 10.1038/ncomms4361
29. Pearl LH, Schierz AC, Ward SE, Al-Lazikani B, Pearl FM. Therapeutic opportunities within the DNA damage response. Nat Rev Cancer. 2015; 15(3):166–80. DOI: 10.1038/nrc3891 [PubMed: 25709118]
30. Reich M, Liefeld T, Gould J, Lerner J, Tamayo P, Mesirov JP. GenePattern 2.0. Nat Genet. 2006; 38(5):500–1. DOI: 10.1038/ng0506-500 [PubMed: 16642009]
31. Ciriello G, Gatza ML, Beck AH, Wilkerson MD, Rhie SK, Pastore A, et al. Comprehensive Molecular Portraits of Invasive Lobular Breast Cancer. Cell. 2015; 163(2):506–19. DOI: 10.1016/j.cell.2015.09.033 [PubMed: 26451490]
32. Cerami E, Gao J, Dogrusoz U, Gross BE, Sumer SO, Aksoy BA, et al. The cBio Cancer Genomics Portal: An Open Platform for Exploring Multidimensional Cancer Genomics Data. Cancer Discovery. 2012; 2(5):401–4. DOI: 10.1158/2159-8290.cd-12-0095 [PubMed: 22588877]
33. Cancer Genome Atlas N. Comprehensive molecular portraits of human breast tumours. Nature. 2012; 490(7418):61–70. DOI: 10.1038/nature11412 [PubMed: 23000897]
34. Bruna A, Rueda OM, Greenwood W, Batra AS, Callari M, Batra RN, et al. A Biobank of Breast Cancer Explants with Preserved Intra-tumor Heterogeneity to Screen Anticancer Compounds. Cell. 2016; 167(1):260–74 e22. DOI: 10.1016/j.cell.2016.08.041 [PubMed: 27641504]
35. Grossman RL, Heath AP, Ferretti V, Varmus HE, Lowy DR, Kibbe WA, et al. Toward a Shared Vision for Cancer Genomic Data. The New England journal of medicine. 2016; 375(12):1109–12. DOI: 10.1056/NEJMp1607591 [PubMed: 27653561]
36. Golub TR, Slonim DK, Tamayo P, Huard C, Gaasenbeek M, Mesirov JP, et al. Molecular Classification of Cancer: Class Discovery and Class Prediction by Gene Expression Monitoring. Science. 1999; 286(5439):531–7. DOI: 10.1126/science.286.5439.531 [PubMed: 10521349]
37. Kummar S, Kinders R, Gutierrez ME, Rubinstein L, Parchment RE, Phillips LR, et al. Phase 0 clinical trial of the poly (ADP-ribose) polymerase inhibitor ABT-888 in patients with advanced malignancies. Journal of clinical oncology : official journal of the American Society of Clinical Oncology. 2009; 27(16):2705–11. DOI: 10.1200/JCO.2008.19.7681 [PubMed: 19364967]
38. Puhalla S, Beumer JH, Pahuja S, Appleman LJ, Tawbi HA-H, Stoller RG, et al. Final results of a phase 1 study of single-agent veliparib (V) in patients (pts) with either BRCA1/2-mutated cancer (BRCA+), platinum-refractory ovarian, or basal-like breast cancer (BRCA-wt). 2014; Chicago. J Clin Oncol. 2014; 32:5s. (suppl; abstr 2570).
39. Fong PC, Boss DS, Yap TA, Tutt A, Wu P, Mergui-Roelvink M, et al. Inhibition of poly(ADP-ribose) polymerase in tumors from BRCA mutation carriers. The New England journal of medicine. 2009; 361(2):123–34. DOI: 10.1056/NEJMoa0900212 [PubMed: 19553641]
40. de Bono JS, Mina LA, Gonzalez M, Curtin N, Wang E, Henshaw JW, et al. First-in-human trial of novel oral PARP inhibitor BMN 673 in patients with solid tumors. 2013; Chicago. J Clin Oncol. 2013; 31 (suppl; abstr 2580).
41. Yang W, Soares J, Greninger P, Edelman EJ, Lightfoot H, Forbes S, et al. Genomics of Drug Sensitivity in Cancer (GDSC): a resource for therapeutic biomarker discovery in cancer cells.

Nucleic Acids Research. 2013; 41(D1):D955–D61. DOI: 10.1093/nar/gks1111 [PubMed: 23180760]

42. Tice RR, Agurell E, Anderson D, Burlinson B, Hartmann A, Kobayashi H, et al. Single cell gel/comet assay: guidelines for in vitro and in vivo genetic toxicology testing. Environ Mol Mutagen. 2000; 35(3):206–21. [PubMed: 10737956]
43. Shen J, Peng Y, Wei L, Zhang W, Yang L, Lan L, et al. ARID1A Deficiency Impairs the DNA Damage Checkpoint and Sensitizes Cells to PARP Inhibitors. Cancer Discovery. 2015; doi: 10.1158/2159-8290.cd-14-0849
44. Johnson SF, Cruz C, Greifenberg AK, Dust S, Stover DG, Chi D, et al. CDK12 Inhibition Reverses De Novo and Acquired PARP Inhibitor Resistance in BRCA Wild-Type and Mutated Models of Triple-Negative Breast Cancer. Cell Rep. 2016; 17(9):2367–81. DOI: 10.1016/j.celrep.2016.10.077 [PubMed: 27880910]
45. Prat A, Karginova O, Parker JS, Fan C, He X, Bixby L, et al. Characterization of cell lines derived from breast cancers and normal mammary tissues for the study of the intrinsic molecular subtypes. Breast cancer research and treatment. 2013; 142(2):237–55. DOI: 10.1007/s10549-013-2743-3 [PubMed: 24162158]

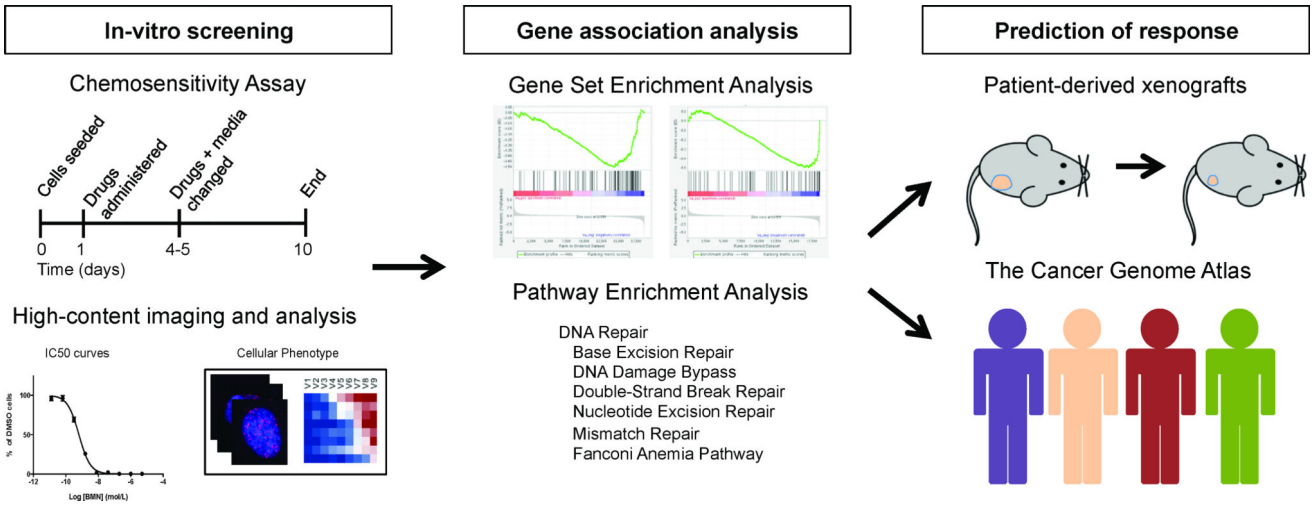

Figure 1.

Workflow of identification of genes and pathways associated with 53BP1 response to PARP inhibition.

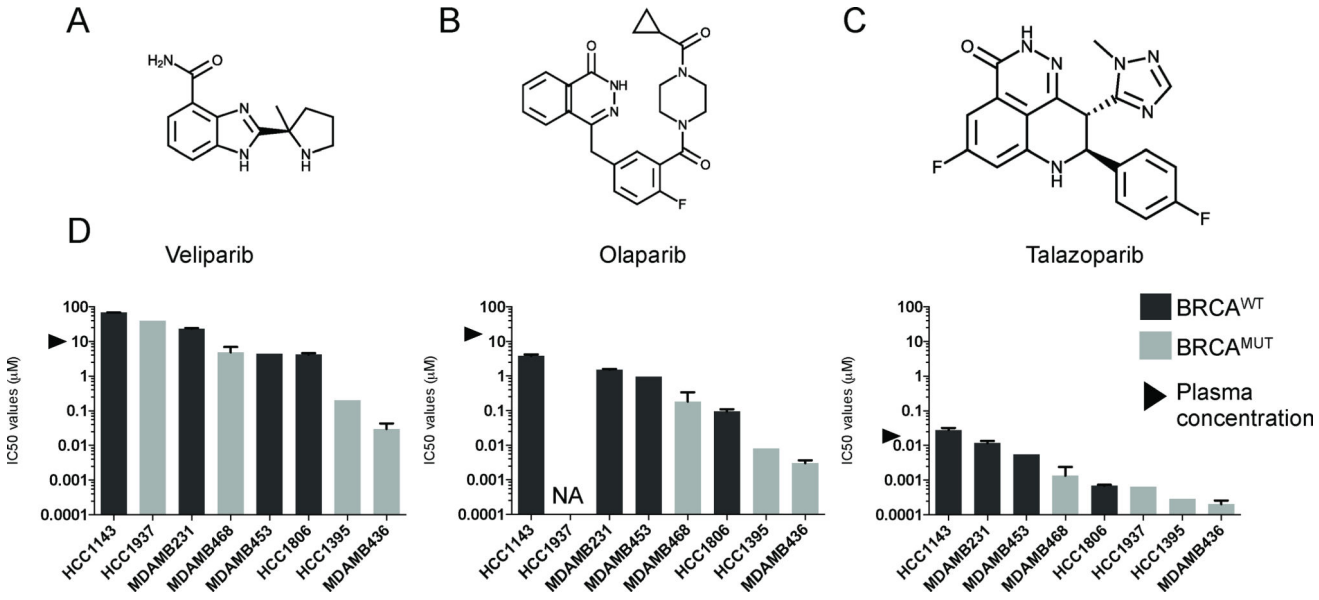

Figure 2.

Chemical structures of **A**, veliparib, **B**, olaparib, **C,** talazoparib. **D**, IC50 values for veliparib, olaparib, and talazoparib compiled for 8 breast cancer cell lines. Average values for triplicate wells and replicate assays were used. Error bars refer to standard error of the mean of replicate assays. Light grey bars refer to BRCA-mutant cell lines, while dark grey bars refer to BRCA wild-type cell lines. Grey arrows refer to plasma concentrations of the PARP inhibitors achieved in patients. N/A refers to not available.

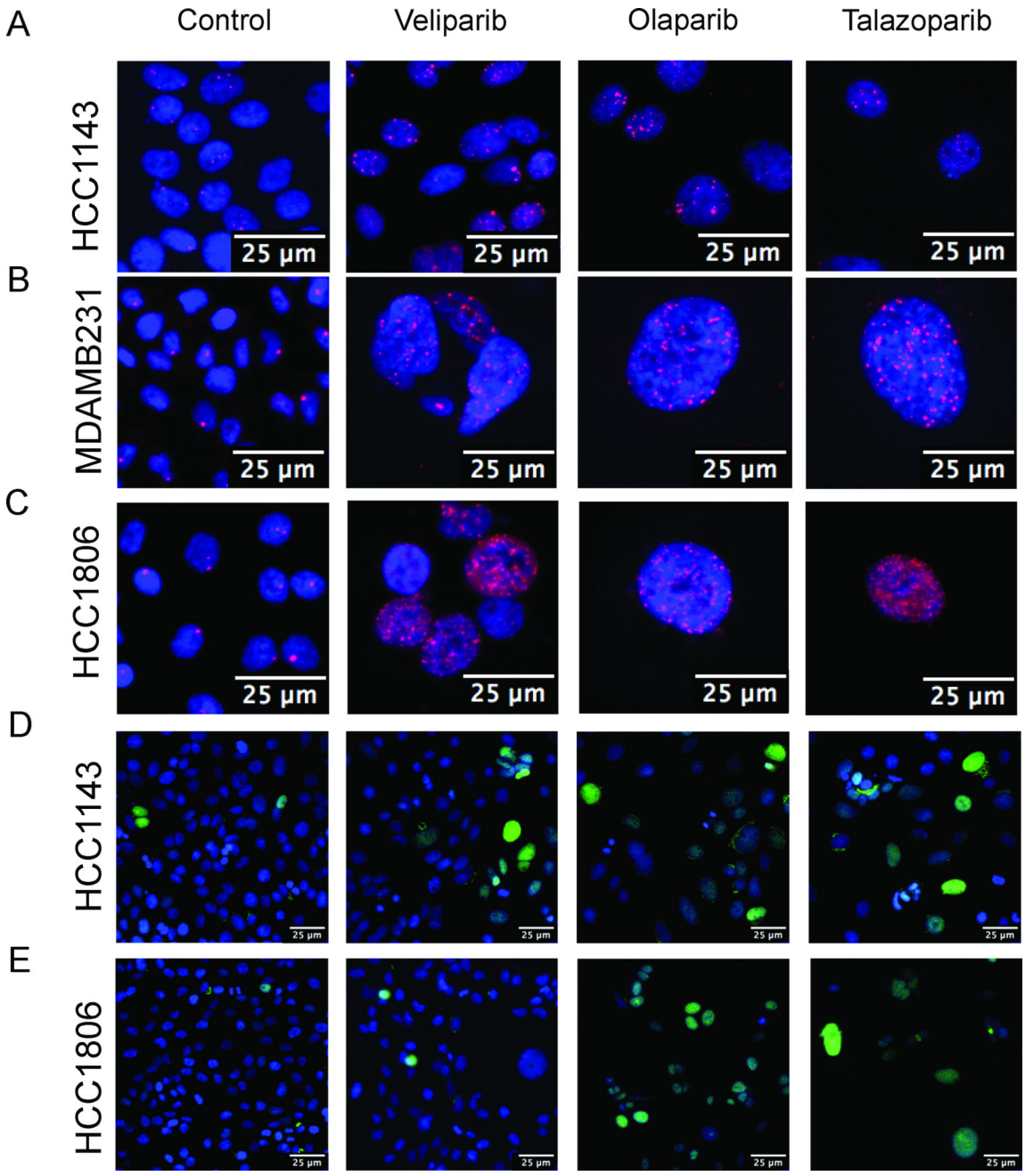

Figure 3.

Cleaved-PARP and 53BP1 expression. Representative images with 10× objective from high-content imaging of control cells in the left column, and cells treated with veliparib, olaparib, and talazoparib in three right columns. 53BP1 expression is seen in: **A**, HCC1143; **B**, MDAMB231; and **C**, HCC1806. Blue represents nuclear staining and pink foci represent 53BP1 foci. Cleaved-PARP expression is seen in **D**, HCC1143 and **E**, HCC1806. Blue represents nuclear staining and green represents cleaved-PARP expression.

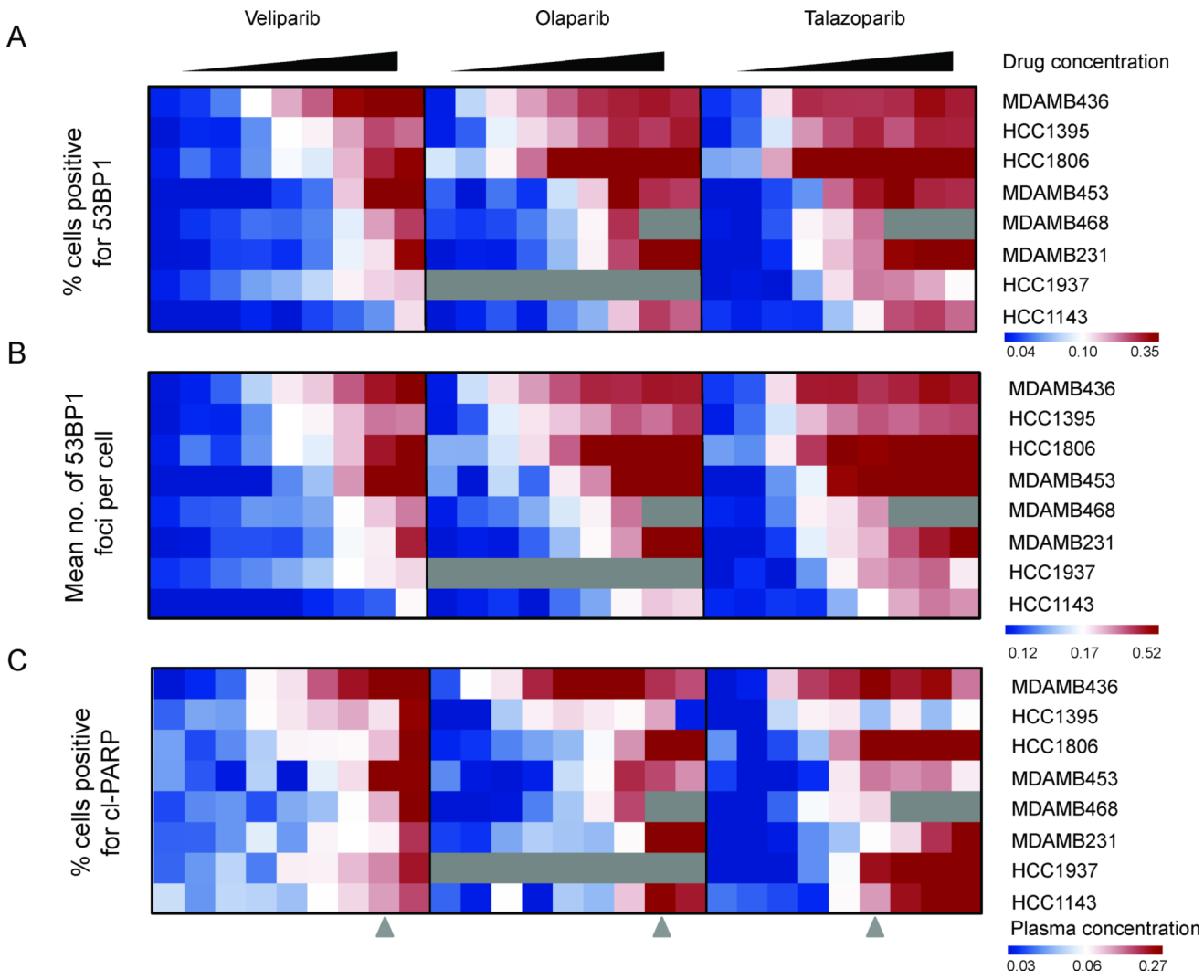

Figure 4.

Heatmap of PARP inhibitors and cellular phenotype. Along the x-axis are nine increasing concentrations of each PARP inhibitor, and along the y-axis are eight different cell lines. Three metrics visualized are: **A**, percentage cells positive for 53BP1; **B**, mean number of 53BP1 foci per cell; and **C**, percentage of cells positive for cleaved-PARP. Grey arrows refer to peak plasma concentrations of the PARP inhibitors achieved in patients.

Table 1

Summary of enriched pathways associated with 53BP1 response.

Reactome Pathway (Major, Minor)	Pathway Proteins	Gene Set Proteins	P-value	FDR	Hit Genes
Cell Cycle	500	40	1.11E-16	1.47E-14	
Cell Cycle Checkpoints	149	18	1.98E-12	9.52E-11	RFC4,PSMA6,RFC2,MRE11A,ANAPC10, CHEK1,RNF168,BRCA1,NBN,TP53,MCM2, MCM3,MCM5,MCM6,SUMO1,PSMD14, PSMD12,BARD1
Cell Cycle, Mitotic	399	25	9.39E-11	2.44E-09	KNTC1,ESCO2,RFC4,PSMA6,RFC2,ZWINT,ANAPC10,POLE2,GINS2,GINS3,GINS4, DHFR,PCNA,SEH1L, PRKCA,MCM2,MCM3,MCM5,MCM6,RRM2,TYMS,BUB1,FEN1, PSMD14,PSMD12
Chromosome Maintenance	64	6	2.56E-04	2.44E-03	RFC4,RFC2,POLE2,PCNA,FEN1,TERF1
Meiosis	63	10	1.80E-08	3.75E-07	RAD51C,MND1,BLM,MRE11A,BRCA1,NBN,PSMC3IP,RAD51,TOP3A,TERF1
DNA Repair	258	32	1.11E-16	1.47E-14	
Base Excision Repair	31	8	1.30E-08	2.86E-07	LIG3,POLB,RFC4,RFC2,TDG,PCNA,UNG, FEN1
DNA Damage Bypass	44	4	3.18E-03	0.0191	USP1,RFC4,RFC2,PCNA
DNA Double-Strand Break Repair	44	7	2.68E-06	4.29E-05	MRE11A,RNF168,BRCA1,NBN,TP53, SUMO1,BARD1
Nucleotide Excision Repair	102	8	8.15E-05	8.66E-04	LIG3,RFC4,RFC2,PCNA,INO80D,XPA, POLR2D,SUMO1
Mismatch Repair	15	3	1.18E-03	8.62E-03	PCNA,EXO1,MSH2
Fanconi Anemia Pathway	36	3	0.0133	0.0624	USP1,FANCE,FANCC
Programmed Cell Death	154	6	0.0189	0.0756	MLKL,PSMA6,TP53,DAPK1,PSMD14,PSMD12

Table 2

Performance of gene signatures in a PDX model and triple-negative breast cancer patients

	Response to Olaparib in PDX (n=7)						TCGA (n=82)
Gene signatures	**Acc**	**Sens**	**Spec**	**PPV**	**NPV**	**Positive test**	**Positive Test**
Combined PARP inhibitor	0.86	0.75	1.00	1.00	0.75	0.43	0.45
Olaparib (Bajrami et al.) (24)	0.71	0.50	1.00	0.50	0.60	0.29	0.49
Talazoparib (Shen et al.) (25)	0.71	0.75	0.67	0.75	0.67	0.43	0.41
HRD Deficiency (Peng et al.) (28)	0.71	0.50	1.00	0.50	0.60	0.29	0.29
Olaparib (Daemen et al.) (20)	0.57	0.25	1.00	1.00	0.50	0.14	0.48
BRCAness (Konstantinopoulos et al.) (26)	0.57	0.75	0.33	0.60	0.50	0.71	0.78
BRCA2MUT (Larsen et al.) (27)	0.43	0.50	0.33	0.50	0.33	0.57	0.68
BRCA1MUT (Larsen et al.) (27)	0.29	0.50	0.00	0.40	0.00	0.71	0.51

Abbreviations: Acc, overall accuracy; Sens, sensitivity; Spec, specificity; PPV, positive predictive value, NPV, negative predictive value.